The Egyptian Journal of Remote Sensing and Space Sciences (2015) 18, 217–233

HOSTED BY

National Authority for Remote Sensing and Space Sciences

The Egyptian Journal of Remote Sensing and Space Sciences

www.elsevier.com/locate/ejrs
www.sciencedirect.com

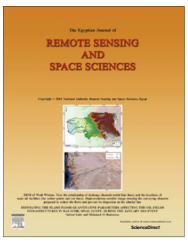

RESEARCH PAPER

Improved Land-use/Land-cover classification of semi-arid deciduous forest landscape using thermal remote sensing

Suman Sinha [a,*], **Laxmi Kant Sharma** [b], **Mahendra Singh Nathawat** [c]

[a] *INSPIRE Fellow (DST-GoI), Department of Remote Sensing, Birla Institute of Technology, Mesra, Ranchi 835215, Jharkhand, India*
[b] *Centre for Land Resource Management, Central University of Jharkhand, Brambe, Ranchi 835205, India*
[c] *School of Sciences, Indira Gandhi National Open University (IGNOU), Maidan Garhi, New Delhi 110068, India*

Received 3 December 2014; revised 11 August 2015; accepted 21 September 2015
Available online 19 October 2015

KEYWORDS

Land Use Land Cover (LULC);
Classification;
Landsat ETM+;
Land surface temperature (LST);
Thermal Vegetation Index (TVI);
Land surface features

Abstract Land Use Land Cover (LULC) change detection helps the policy makers to understand the environmental change dynamics to ensure sustainable development. Hence, LULC feature identification has emerged as an important research aspect and thus, a proper and accurate methodology for LULC classification is the need of time. In this study, Landsat-7 satellite data captured by Enhanced Thematic Mapper (ETM+) were used for LULC classification employing the maximum likelihood supervised classification (MLC) algorithm. The study targets the improvement of classification accuracy with the combined use of thermal and spectral information from satellite imagery. Land surface temperature (LST) is sensitive to land surface features and hence can be used to extract information on LULC features. The classification accuracy was found to improve on integrating the thermal information from the thermal band of Landsat ETM+ with spectral information. Two thermal vegetation indices, namely Thermal Integrated Vegetation Index (TLIVI) and Advanced Thermal Integrated Vegetation Index (ATLIVI), proposed in this study showed fairly good correlations (R^2 = 0.65 and 0.7, respectively) with the derived surface temperature. These indices based on empirical parameterization of the relationship between surface temperature (T_s) and vegetation indices showed an increase of nearly 6% in the overall accuracy for land-use/land-cover (LULC) classification in comparison to MLC algorithm using Standard False Colour Composite (FCC) satellite image of Landsat ETM+ as reference.

1. Introduction

Land Use Land Cover (LULC) dynamics serves as a crucial parameter in current strategies and policies for natural resource management and monitoring. Currently, the world

* Corresponding author.
E-mail address: sumanrumpa.sinha@gmail.com (S. Sinha).
Peer review under responsibility of National Authority for Remote Sensing and Space Sciences.

http://dx.doi.org/10.1016/j.ejrs.2015.09.005
1110-9823

has witnessed the importance of LULC changes in world-wide environmental modifications that can lead to adverse effects (Iqbal and Khan, 2014). Changes in LULC signify environmental changes brought about by natural or anthropogenic consequences (Rawat and Kumar, 2015). This provides an important aspect in evaluating, monitoring and conserving Earth's resources that is required for sustainable development and economic proliferation of an area (Rawat et al., 2013a). Rational use of the available land is important for sustainable conservation of the bio-environment which ultimately improves the socio-economic status for a sustainable livelihood. This requires the accurate estimation of the present and past LULC dynamics. With the advent and development of the integrated geospatial techniques that integrate the use of Remote Sensing (RS), Geographic Information Systems (GIS) and Global Positioning System (GPS), the enumeration of spatio-temporal LULC dynamics has become easy, quick, cost-effective and accurate (Rawat and Kumar, 2015). Digital image processing on multi-temporal multi-spectral satellite imagery has great potential in LULC categorization, landscape dynamics and change detection analyses. The digital classification techniques include the unsupervised (K-means and ISODATA), supervised and object-based classification; out of which the most commonly used classification technique is the supervised classification technique (Enderle and Weih, 2005); however, object-based classification has shown better accuracy (Blaschke, 2010). Furthermore, object-based classification is possible with the use of high spatial resolution of the satellite imagery. Often, in cases of spectral mixtures, a hybrid classification is used for distinguishing land features (Kumar et al., 2013). On the other hand, classification accuracy can be improved by using multi-source data (Nizalapur, 2008; Li et al., 2011). Land surface temperature (LST) estimated from the remotely sensed thermal band shows unique response to landscape dynamics involving LULC changes (Weng et al., 2004; Setturu et al., 2013; Hussain et al., 2014). Hence, thermal infrared (TIR) sensors can determine quantitative information of surface temperature across different LULC categories (Sinha et al., 2014).

Intricate relationships exist between LST and several physico-chemical and biological processes of the Earth (Becker and Li, 1990). Hence, LST acts as a key parameter in the physics of land surface processes, surfaces–atmosphere interactions and energy fluxes between the ground and the atmosphere because it is involved in the energy balance (Sobrino et al., 2003). Hence, it can provide important information about the surface physical properties and climate which plays a role in many environmental processes (Dousset and Gourmelon, 2003; Weng et al., 2004) and is thus of great interest for meteorological and climatological studies. On the other hand, the climate is altered due to changes in LULC and anthropogenic activities. Detailed explanation of the physics and theory behind deriving LST is conceptualized in Dash et al. (2001, 2002). Satellite remote sensing is probably the best way to retrieve this parameter both regionally and globally due to the availability of high resolution, consistent and repetitive coverage and capability of measurements of earth surface conditions (Owen et al., 1998). Tomlinson et al. (2011) has made a detailed review of the role of remote sensing technology in LST for meteorology and climatology and also mentioned the different thermal remote sensing sensors providing immense potentially useful datasets to measure LST.

LST being sensitive to vegetation and soil moisture; can be used to detect changes in land use/land cover features (Mallick et al., 2008). Extensive studies using MODIS for LST retrieval are present revealing good results for small-scale global scenario (Galve et al., 2007; Pinheiro et al., 2007; Hanes and Schwartz, 2011; van Leeuwen et al., 2011; Mildrexler et al., 2011; Hachem et al., 2012; Bayala and Rivas, 2014). Several studies are carried out for the retrieval of LST from Landsat Thematic Mapper (TM) and ETM+ thermal data; which is better for large-scale regional and local set-up (Alavipanah et al., 2007; Yue et al., 2007; Mallick et al., 2008; Bayala and Rivas, 2014; Hussain et al., 2014). Thermal infrared band (10.44–12.42 μm) present in TM/ETM+ with high spatial resolution (120 m for TM and 60 m for ETM+) is much useful for local and regional thermal infrared study. In order to achieve a high accuracy in prediction of LST from TM/ETM+ thermal data with fewer parameters it is necessary to develop new methods that are robust and easily applied.

One of the important aspects in radiance balance and transfer is the surface emissivity. The surface of the Earth comprises of varied and complicated land-use and land-cover feature types and accurate measurements of the surface emissivities of these features are not easy. Based on the conventional land cover classification including dynamic and seasonal factors, Snyder et al. (1998) gave a detailed classification of emissivity using MODIS thermal infrared bands. On the other hand, vegetation indices, like Normalized Difference Vegetation Index (NDVI), Soil Adjusted Vegetation Index (SAVI) and Leaf Area Index (LAI) can be used as an alternative for the estimation of surface temperature (Faris and Reddy, 2010). Apparent correlation exists between LST and NDVI (Kaufmann et al., 2003; Yue et al., 2007) and varies with land cover changes (Julien et al., 2011). Correlations between LST and NDVI vary seasonally and diurnally (Sun and Kafatos, 2007). LAI being one of the most important biophysical and biochemical factors of the land cover also bears relationship with the surface temperature (Jin and Zhang, 2002). A new model of Light Use Efficiency (LUE) estimation has been proposed using three VIs, including NDVI, EVI2 (Enhanced Vegetation Index) and SAVI, in association with scaled LST indicates moderate estimates of LUE using MODIS (Wu and Niu, 2012).

With the advent of new climate agreements like REDD (Reducing Emissions from Deforestation and Degradation), there has been an ever-increasing demand for accurate forest monitoring methods (Sharma et al., 2013; van Leeuwen et al., 2011). ETM+ thermal data can be used to estimate the temperatures inside a forest, which is impossible with conventional methods. This can be used to determine the canopy surface temperature or the forest surface temperature (FST). The variation in the thermal response for vegetation is a function of the biophysical properties of the vegetation (Weng, 2009). The present study analyses the potential of thermal information from Landsat-7 ETM+ for LULC classification over heterogeneous tropical forest area. The main objective of the study is to propose an index generated using both thermal and spectral information from satellite imagery for improvement in the accuracy of LULC classification. Spatial analysis was carried out by building models involving vegetation spectral indices like NDVI, SAVI and LAI with surface emissivity to estimate the surface temperature and two Thermal vegetation indices were developed in this study that integrated NDVI, LAI and EVI2 with Landsat-7 ETM+ TIR

band 6 information. Landsat 7 was used as it collects thermal data with highest spatial resolution (60 m at nadir) currently available through remote sensing of space. There existed a potential relationship between the surface features and the LST (Sinha and Sharma, 2013). Relevant studies were done using the integration of surface temperature and vegetation indices mainly NDVI for land cover mapping (Lambin and Ehrlich, 1995, 1996; Sandholt et al., 2002; Wan et al., 2004; Julien et al., 2011).

2. Materials and methods

2.1. Study area and datasets

Sariska Wildlife Reserve situated in Rajasthan, India was selected as a case study and is shown in Fig. 1. Satellite data of Landsat ETM+ of 2006 were downloaded from GLCF (http://glcf.umiacs.umd.edu). Survey of India toposheets were also used for classifying the land use and land cover along with the satellite imagery. The study area is a protected area of the reserve situated among the Aravali hill ranges covering an area of nearly 1183 km^2. The area has limited anthropogenic interventions.

2.2. Image interpretation for LULC

The Landsat ETM+ image was co-registered and geometrically rectified in reference to the SOI toposheets (scale 1:50,000). The image was checked with the distinct identifiable objects on the ground. Spectral information was used to correlate image characteristics and ground features as a standard visual technique. The spectral signatures for different land use and land cover types were established and False-Colour Composite (FCC) was interpreted based on image elements. Ground truth was collected from study area to identify different elements. Tonal and textural variations due to altitude dependent vegetation and contour information from toposheet were made use of during interpretation. The image was processed for classification of the different features on the ground. For supervised classification using maximum

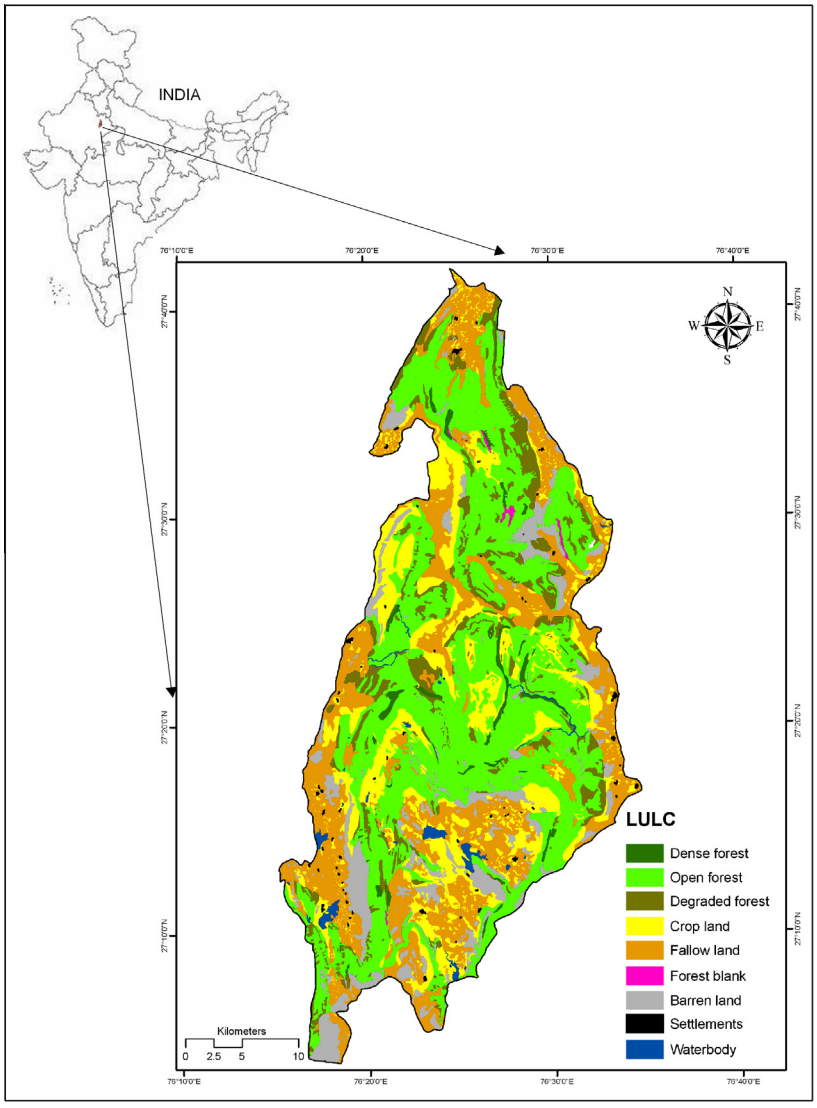

Figure 1 Land-use/land-cover classification map of the study area of Sariska Wildlife Reserve (India).

likelihood supervised classification (MLC) algorithm, training sets were selected in the FCC imagery with three bands of green (2), red (3) and near-infrared (4) based on the collected sample points for respective LULC classes (Sinha et al., 2011a,b). Training sites for LULC classification were selected based on knowledge developed through extensive ground survey and detailed field study of the area; along with the topographical sheets and IRS P6 LISS III image of the study area was taken into account. The training sites were proportionately selected comprising of pure pixels. 100 random points were generated as sample points that were cross-checked using GPS in the field. Fig. 1 shows the LULC classification of the study area.

2.3. Spectral vegetation indices

Remote sensing spectral indices were applied for better classification results (El-Asmar et al., 2013; Rawat et al., 2013a,b; Rawat and Kumar, 2015). In this study, the NDVI and LAI were calculated from visible and near infrared bands of ETM + imagery following Eqs. (1–3). Band 4 corresponds to near infra-red (NIR) and band 3 for Red (R) bands in ETM +. To calculate and get the image of LAI, first the SAVI was calculated. SAVI is suitable for regions with low vegetation cover and a consequently higher percentage of soil reflectance (Jenerette et al., 2007); hence, needs to be calculated first (Eq. 2). In this equation, L is a constant whose value depends on the soil properties and $L \approx 0.5$. The LAI is calculated from the empirical equation (Faris and Reddy, 2010) that is related to SAVI as mentioned in Eq. (3).

EVI, as proposed by Huete et al. (1997) involves the use of blue band to primarily account for atmospheric correction and variable soil and canopy background reflectance. Unswervingly, the index normalizes the reflectance in red band as a function of the reflectance in the blue band. This is effectively used for estimating forest terrestrial variables (Zhang et al., 2003; Sims et al., 2008). The calculation of EVI is mentioned in Eq. (4), where NIR, R and B are surface reflectance in near-infrared, red and blue spectral bands respectively; G is gain factor; C_1 and C_2 are coefficients of aerosol resistance and L is a canopy background adjustment, that functions as soil-adjusted factor as in SAVI (Eq. (3)), the value being different from the L in SAVI due to the interactions between the soil adjusted factor and the aerosol resistance terms (Liu and Huete, 1995; Jiang et al., 2008). Jiang et al. (2008) proposed a two-band EVI (EVI2) without a blue band and found that the EVI2 could be a good proxy of EVI while less dependent on band design and modified as Eq. (5).

2.4. Retrieval of surface temperature and associated parameters

In remote sensing, retrieval of LST is based on Planck's law which states the dependence of spectral radiance (L_λ) at a certain spectral band with wavelength λ emitted from a blackbody (i.e., surface emissivity $\varepsilon(\lambda) = 1$) on the body's kinetic temperature (Mildrexler et al., 2011). The black body temperature at satellite or at-sensor brightness temperature (T_b) is first calculated for estimating the surface temperature (Weng et al., 2004; Fan et al., 2007; NASA, 2008; Sinha et al., 2014; Sinha, 2015). The calibration for Thermal band data of band 6 is performed following a two-step process (Landsat Project Science Office, 2002; Sinha et al., 2014; Sinha, 2015). First step involves the conversion of band 6 digital number (DN) values into L_λ ($W\,m^{-2}\,sr^{-1}\,\mu m^{-1}$) (NASA, 2009). Secondly, this L_λ is converted to T_b in Kelvin (Weng et al., 2004; Stathopoulou and Cartalis, 2007; Fan et al., 2007; NASA, 2008; Faris and Reddy, 2010; Sinha et al., 2014; Sinha, 2015).

Next, the emissivity correction is carried out using surface emissivities for the specified land covers estimated from the NDVI (Eq. 1) and LAI (Eqs. (2 and 3)) values (Bastiaanssen et al., 1998; Oberg and Assefa, 2006; Duah et al., 2008; Faris and Reddy, 2010) as mentioned in Eq. (6). Numerous literature documents the steps involved in the computation of emissivity corrected land surface temperature T_s (Weng et al., 2004; Weng and Yang, 2006; Stathopoulou and Cartalis, 2007; Faris and Reddy, 2010; Sinha et al., 2014; Sinha, 2015). An additional correction for atmospheric interference is also required for accurate estimation of surface temperature. Error in the emissivity correction is two times larger than the error in the atmospheric correction in the estimation (Prata et al., 1995); and as we are interested in relative surface temperature differences between different Land Use Land Cover features, the error due to the atmospheric interferences is not taken into account. Albedo, being an important parameter affecting the derivation of surface temperature (Price, 1989), has been used in several studies to derive LST (Buermann et al., 2001; Wen et al., 2003; Hales et al., 2004; Peña, 2009; Faris and Reddy, 2010; Wang et al., 2011). Albedo was retrieved using the reflectance bands from Landsat data according to the following conversion formula (Peña, 2009) mentioned in Eq. (7) 7. Fractional vegetation cover (F_c) which is also a significant factor in surface temperature and used in several studies (Li et al., 2004; Mallick et al., 2008; Glenn et al., 2008; Wang et al., 2011; Mildrexler et al., 2011), was determined using Eq. (8). These parameters were investigated and only those were selected which could show the greatest potential and response in distinguishing the different LULC categories. Due to the unique response of LST towards the different LULC types, the thermal information from which LST was calculated was used as an input of the new indices developed in the study for LULC classification. Finally, the selected spectral and thermal information were integrated to develop two new indices that were used for LULC classification.

In our study, an index is derived based on two additional parameters of NDVI and LAI along with DN band 6 ETM + information, known as TLIVI (Thermal Integrated Vegetation Index) and mentioned in Eq. (9). As observed in this study and also discussed in the forthcoming section, EVI2 shows a better correlation with derived LST as compared to NDVI and LAI. Hence, another index is formulated based on this additional parameter of EVI2 integrated to TLIVI as an advancement of TLIVI, known as ATLIVI (Advanced Thermal Integrated Vegetation Index) and is observed to serve better for LULC classification and is mentioned in Eq. (10). Both TLIVI and ATLIVI are integrated with NIR and Red bands of ETM + to construct a FCC that is used as the reference for supervised classification. The accuracy for the classifications is measured and compared to that with Standard FCC. The steps of the entire methodology are shown in Fig. 2. All the formulae mentioned and used in the study are concise in Table 1.

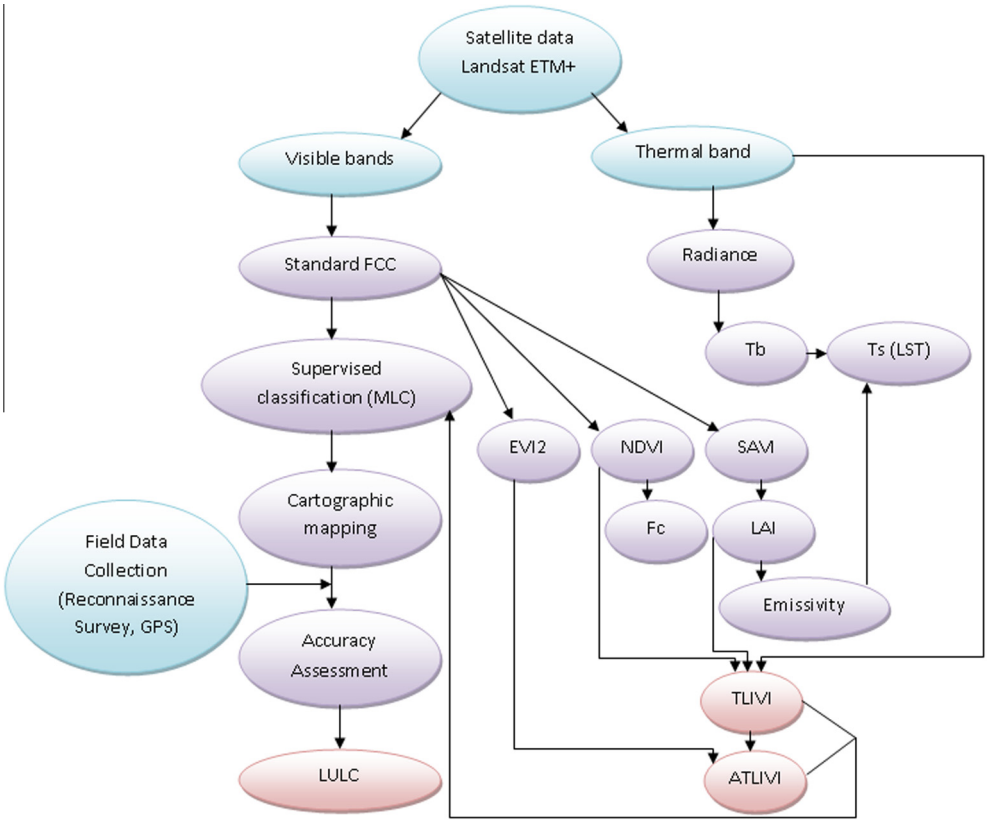

Figure 2 Methodology flow-diagram.

3. Results and discussion

3.1. LULC feature interpretation

Fig. 1 shows the following LULC features classified, namely, open forest (OF), dense forest (DF), degraded forest (DDF), forest blank (FB), fallow land (FL), crop land (CL), barren land (BL), waterbody (WB), settlement (ST). These different land features responded to thermal band uniquely due to the difference in their emissivity properties. This depended on the relative proportions of chlorophyll, soil and moisture content in the respective LULC features. Consequently, the indices used in the study also behaved accordingly and showed different responses depending on the different LULC features; since, all the indices were developed using spectral (optical and thermal) band information. Weng (2009) had documented numerous instances where thermal information and LST show a relationship with surface bio-physical characteristics, preferably, vegetation indices which in turn varied with different LULC features.

3.2. Retrieval of surface temperature parameters

Using Landsat-7 ETM+ imagery (Fig. 1), various spatial parameters like NDVI, SAVI, LAI, EVI2, Surface Emissivity, LST and LULC map related to heterogeneous tropical forests of Sariska Wildlife Reserve were computed (Figs. 1, 3 and 4). LULC classification resulted in the formation of different Land feature classes as shown in Fig. 1. Accuracy assessment performed for this classification showed an overall accuracy of 85.8% and Kappa accuracy of 0.81. The spatial variation of NDVI (Fig. 3a) ranged from values less than 0 (0 to −0.5) at area of no vegetation cover and water bodies to 0.5 at area covered by high density of vegetation cover. The spatial distribution of LAI (Fig. 3b) showed that, the values were ranged from negative values of −1.15 at the water bodies to positive values of as high as 6–7 at areas characterized by vegetation. Emissivity is directly related to NDVI and LAI values and in terms of spatial distribution; it showed similar trends as NDVI and LAI (Fig. 3d). EVI2, in spatial context (Fig. 3c) showed higher values of nearly 0.15 on an average for the dense vegetated regions, while an average value of −0.03 in the barren and uncovered areas was obtained. The spatial distribution of surface temperature in Sariska and surrounding areas varied between nearly 27 °C at water bodies and 25 °C in the vegetation areas in the minimum scale to a maximum of 37–39 °C for fallow and barren open spaces, concrete surfaces, bare soils and rocky wastes (Fig. 4). Hence, the temperature difference among different LULC classes reached nearly 14 °C. LULC (Fig. 1), as derived from Landsat-7 ETM + imagery, is the focal surface feature parameter controlling the spatial variation of land surface temperature.

The forests of Sariska were dry and deciduous with open forests covering the maximum extent and having small heterogeneously distributed patters of settlements with limited anthropogenic activities in context to alteration of natural surface characteristics. Several agricultural fields were scat-

Table 1 Formulae used to calculate remote sensing-based spectral indices.

Eqs.	Formula	References	Remarks
1	$\mathrm{NDVI} = \frac{(\mathrm{NIR}-\mathrm{R})}{(\mathrm{NIR}+\mathrm{R})}$	Lillesand and Kiefer (2003)	Surface reflectance in near-infrared (NIR) and red (R) spectral bands
2	$\mathrm{SAVI} = \frac{(\mathrm{NIR}-\mathrm{R})\times(1+L)}{(\mathrm{NIR}+\mathrm{R}+L)}$	Jenerette et al. (2007)	L is a constant whose value depends on the soil properties
3	$\mathrm{LAI} = -\frac{\ln((0.69-\mathrm{SAVI})/0.59)}{0.91}$	Faris and Reddy (2010)	
4	$\mathrm{EVI} = G \times \frac{(\mathrm{NIR}-\mathrm{R})}{(\mathrm{NIR}+C_1\mathrm{R}-C_2\mathrm{B}+L)}$	Huete et al. (1997, 2002), Jiang et al. (2008), Glenn et al. (2008)	Surface reflectance in blue (B) spectral band, $G = 2.5$, $C_1 = 6$, $C_2 = 7.5$, $L = 1$
5	$\mathrm{EVI2} = 2.5 \times \frac{(\mathrm{NIR}-\mathrm{R})}{(\mathrm{NIR}+2.4\times\mathrm{R}+1)}$	Jiang et al. (2008)	
6	$\varepsilon = 0.047^{*}\ln(\mathrm{NDVI}) + 1.009$ $\varepsilon = 0.003^{*}(\mathrm{LAI}) + 0.97$; for LAI < 3.0	Faris and Reddy (2010)	
7	$\alpha_{\mathrm{short}} = 0.356 * \alpha_1 + 0.130 * \alpha_3 + 0.373 * \alpha_4 + 0.085 * \alpha_5 + 0.072 * \alpha_7 - 0.0018$	Peña (2009)	α_{short} is shortwave broadband albedo, and $\alpha_1, \ldots, \alpha_7$ are the reflectance of the respective band number of Landsat ETM+
8	$F_c = 1 - \left(\frac{\mathrm{NDVI}_{\mathrm{scmax}}-\mathrm{NDVI}_i}{\mathrm{NDVI}_{\mathrm{scmax}}-\mathrm{NDVI}_{\mathrm{scmin}}}\right)^{0.625}$	Choudhury et al. (1994), Karnieli et al. (2010)	$\mathrm{NDVI}_{\mathrm{scmax}}$ and $\mathrm{NDVI}_{\mathrm{scmin}}$ are the maximum and minimum NDVI values from the scene and NDVI_i is the NDVI value of ith pixel
9	$\mathrm{TLIVI} = \frac{(\mathrm{DN}_{\mathrm{ETM+band6}}-\mathrm{NDVI}-\mathrm{LAI})}{(\mathrm{DN}_{\mathrm{ETM+band6}}+\mathrm{NDVI}+\mathrm{LAI})}$	In this study	
10	$\mathrm{ATLIVI} = \frac{(\mathrm{DN}_{\mathrm{ETM+band6}}-\mathrm{NDVI}-\mathrm{LAI}-\mathrm{EVI2})}{(\mathrm{DN}_{\mathrm{ETM+band6}}+\mathrm{NDVI}+\mathrm{LAI}+\mathrm{EVI2})}$	In this study	

tered in the surrounding areas. Due to the extreme abundance of vegetation in the area that reduced the radiation heat flux of the earth surface by consuming most of the radiation energy during the evapotranspiration process, the overall surface temperature was reduced as compared to the barren land and pure urban areas. In our study area, ST for water bodies was to some extent high as compared to the vegetation areas. As the settlements were scattered in heterogeneous pockets with the forest regions, there was reduction in the surface temperature due to the impact from vegetation cover. The univariate statistics including minimum, maximum, mean and standard deviation of radiation heat flux parameters for different land use/land cover for the study area were calculated and documented in Table 2. The table also summarizes similar statistics computed for surface emissivity, spectral radiance and different vegetation indices considered in this analysis for the respective LULC categories of the study area. Several other associated parameters, like the albedo, normalized LST and fractional vegetation cover were also enumerated. Retrieval of albedo with Eq. (7) showed greater average values for uncovered barren and settlement areas; low average values for vegetation lands, but least for the water bodies. Fractional vegetation cover as assessed using Eq. (8), depended on NDVI and showed average values of more than 0.5 in forest areas, 0.4 for crop lands and degraded forested areas, whereas average values of 0.3 for fallow and barren lands. Water bodies also showed an average value of 0.3, even less than barren and fallow lands as they had average values of more than 0.35 but less than 0.4. Hence, the water features were distinctly separated, as also revealed in the figures. The clear demarcation of the forested areas was also illustrated from the figures. All the LULC categories confirmed variation in the univariate statistical values of radiation heat flux parameters (Figs. 3 and 4), as documented in Table 2 since these are continuous spatial parameters characterized by gradational change in the values of each parameter. Table 2 shows the range of each parameter under study with their average and standard deviation values.

3.3. Thermal Vegetation Index-LULC classification

LULC is dynamic in nature and its dynamism affects several parameters (Sharma et al., 2012). It is hence observed that surface temperatures are unique characteristics of every LULC classes. So, it was possible to make much more accurate classification for LULC when the parameter of surface temperature was considered. However, using simply the LST or Landsat ETM+ band 6 DN information was not enough to classify. Fig. 4 shows the trend of the ST profile for LULC classes. Open forest, dense forest and forest blank had narrow range of ST that could not be easily distinguished for classification based on ST profiles. On the other hand, settlement and water body had similar ST range. This was purely due to the fact that the settlement areas were un-uniformly randomly distributed in pockets that are near or within the forests. So, probably the effect of low ST of the forests influenced the ST of the settlement areas. Also the settlements were small rural villages with maximum areas covered with dry or moist soil near to small water potholes; hence paved ways and concrete structures were absent. Simultaneously, agricultural lands and degraded forests showed similar trends. Hence, mixed boundary pixels for different classes were observed during extraction processes. Higher resolution imagery could solve out this problem to some extent. These observations revealed that DN of ETM+ thermal band could not serve the purpose of LULC classification alone.

Fig. 5(a and b) shows the map derived from the thermal vegetation indices (TLIVI and ATLIVI respectively). Fig. 6 shows the FCC constructed with ATLIVI, Red and NIR in RGB channels on which the classification was done. Likewise, FCC with TLIVI, Red and NIR in RGB channels was also generated. The same training sites of the respective LULC features were used for classification. Accuracy assessment of LULC classification using ATLIVI as an additional band to form FCC was done to find an overall accuracy (OA) of 91% and Kappa accuracy (k) of 0.87 in comparison

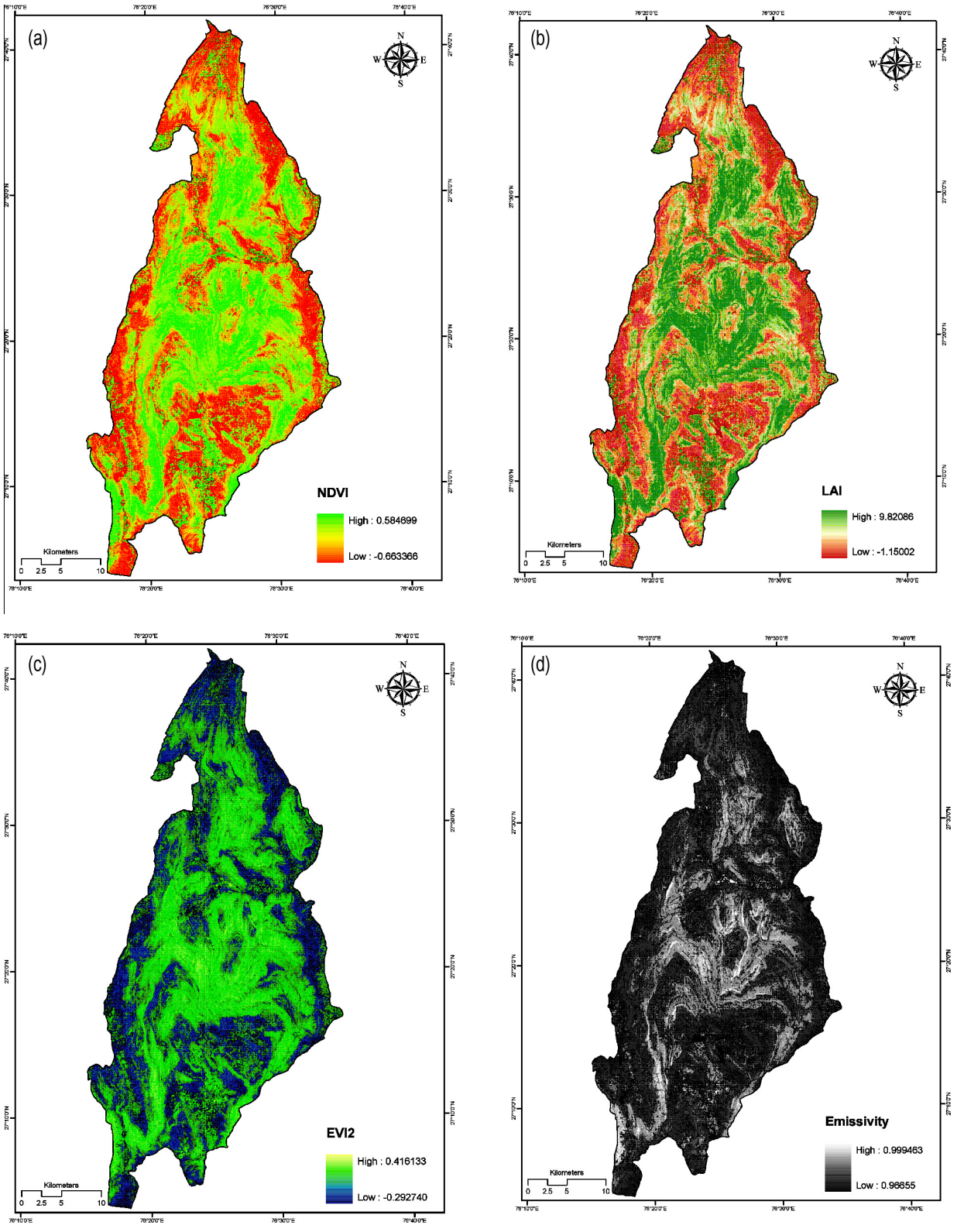

Figure 3 Radiation heat flux and associated vegetation parameters: (a) Normalized Difference Vegetation Index (NDVI) map. (b) Leaf-Area Index (LAI) map. (c) Enhanced Vegetation Index (EVI2) map. (d) Surface emissivity.

to 85% and 0.8 respectively with standard FCC (Fig. 1); even slightly more than that obtained from classifying the map using TLIVI as an additional band to design FCC (OA = 90.2% and k = 0.86) as shown in Table 3. Several other combinations of band 6 DN, ST, NDVI, LAI and EVI2 were tried out but the relation mentioned in Eq. (10)

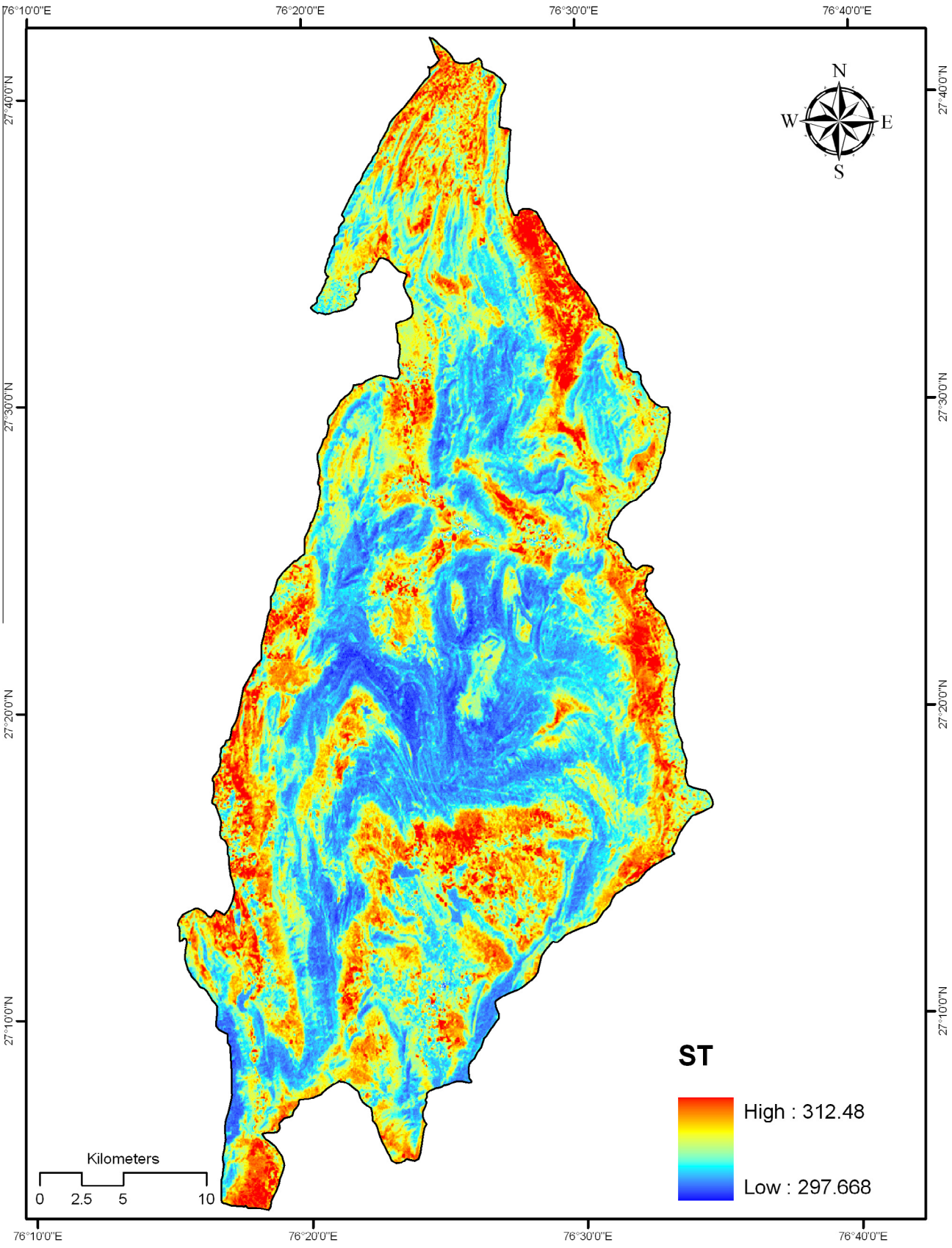

Figure 4 Land surface temperature (LST) in Kelvin.

Table 2 Univariate statistics of radiation heat flux and associated parameters for LULC categories.

	LULC	MIN	MAX	AV	SD
NDVI	Open forest	−0.26666668	0.449664	0.21813079	0.098675
	Fallow land	−0.55102038	0.515152	0.02373323	0.153762
	Crop land	−0.49640289	0.51269	0.06959572	0.120142
	Degraded forest	−0.24293785	0.402439	0.11621217	0.118331
	Barren land	−0.41333333	0.437838	−0.00737266	0.11725
	Dense forest	−0.13089006	0.4375	0.27201155	0.083228
	Waterbody	−0.49425286	0.358974	−0.09951518	0.221777
	Forest blank	−0.14102565	0.365854	0.15099911	0.114971
	Settlement	−0.2568306	0.392265	0.06912051	0.145016
SAVI	Open forest	−0.6813	0.5961	0.15572237	0.165661
	Fallow land	−0.6961	0.8747	0.01540069	0.239751
	Crop land	−0.6183	0.8153	0.09334957	0.168966
	Degraded forest	−0.4545	0.7094	0.14817916	0.183472
	Barren land	−0.618	0.6246	−0.00392601	0.177608
	Dense forest	−0.2114	0.7143	0.40705521	0.119434
	Waterbody	−0.9901	0.6581	−0.14410999	0.33553
	Forest blank	−0.2861	0.5797	0.22989389	0.168417
	Settlement	−0.38419619	0.586777	0.10336161	0.216891
LAI	Open forest	−0.9268	2.0196	0.16716235	0.369918
	Fallow land	−0.9386	7.0976	−0.05608408	0.50089
	Crop land	−0.8751	6.6849	0.04217252	0.395402
	Degraded forest	−0.7282	3.0068	0.16622005	0.419042
	Barren land	−0.8749	2.4172	−0.13351593	0.335685
	Dense forest	−0.4657	3.7041	0.9013532	0.460083
	Waterbody	−1.15	3.2067	−0.26274588	0.552159
	Forest blank	−0.5532	1.8424	0.35051705	0.421762
	Settlement	−0.65846747	1.915637	0.10394701	0.509095
EVI2	Open forest	−0.21626298	0.33867	0.11860720	0.06703
	Fallow land	−0.28218061	0.337838	−0.02397966	0.094884
	Crop land	−0.24080561	0.300875	0.0096312	0.079911
	Degraded forest	−0.2122016	0.318736	0.04947591	0.084403
	Barren land	−0.26682135	0.235294	−0.03698854	0.084017
	Dense forest	−0.11357184	0.266904	0.14507575	0.05406
	Waterbody	−0.19452812	0.245098	0.05069233	0.091641
	Forest blank	−0.12716936	0.250313	0.06618045	0.082742
	Settlement	−0.17596102	0.225904	0.00698014	0.082183
F_c	Open forest	0.20582226	0.71424	0.51759210	0.071659
	Fallow land	0.05551476	0.787558	0.38482506	0.102784
	Crop land	0.08322062	0.784541	0.41316631	0.081771
	Degraded forest	0.21912746	0.667807	0.44494297	0.082018
	Barren land	0.12635256	0.702208	0.36247211	0.07668
	Dense forest	0.28390577	0.701868	0.55855793	0.063113
	Waterbody	0.08432152	0.628288	0.31107541	0.138227
	Forest blank	0.27790397	0.634371	0.46920394	0.080508
	Settlement	0.21132118	0.658313	0.41444002	0.098962
Surface Albedo	Open forest	0.06866559	0.208578	0.13097200	0.01251
	Fallow land	0.06073494	0.214877	0.15237982	0.014488
	Crop land	0.06705828	0.217412	0.14586122	0.014122
	Degraded forest	0.07308157	0.194283	0.1378112	0.016174
	Barren land	0.06939133	0.243618	0.15264409	0.018893
	Dense forest	0.09077237	0.164174	0.13240268	0.011854
	Waterbody	0.04846698	0.186851	0.11277638	0.034595
	Forest blank	0.09964452	0.168812	0.13503548	0.0134
	Settlement	0.11079873	0.203004	0.15183834	0.012109
L_λ	Open forest	8.8329	10.6488	9.347475	0.252358
	Fallow land	8.9071	10.7971	9.82771247	0.298646
	Crop land	8.9071	10.6488	9.6374982	0.263446
	Degraded forest	8.87	10.6118	9.51429716	0.292461
	Barren land	8.9071	10.76	9.75240592	0.305045
	Dense forest	8.87	10.0559	9.21588417	0.17364

(*continued on next page*)

Table 2 (*continued*)

	LULC	MIN	MAX	AV	SD
	Waterbody	8.9071	10.4635	9.41410242	0.366798
	Forest blank	9.0553	10.13	9.44832219	0.19623
	Settlement	9.12940788	10.42647	9.64476794	0.234437
ε	Open forest	0.9672	0.9761	0.97050158	0.001111
	Fallow land	0.9672	0.9913	0.96983132	0.001502
	Crop land	0.9674	0.9901	0.9701264	0.001187
	Degraded forest	0.9678	0.979	0.97049879	0.001258
	Barren land	0.9674	0.9773	0.96959922	0.001008
	Dense forest	0.9686	0.9811	0.97270507	0.00138
	Waterbody	0.9665	0.9796	0.96921144	0.001657
	Forest blank	0.9683	0.9755	0.97105144	0.001265
	Settlement	0.96802461	0.975747	0.97031184	0.001527
ST (T_s in K)	Open forest	298.6441	310.6456	302.591017	2.045389
	Fallow land	299.2168	312.48	305.670956	2.420612
	Crop land	298.44	311.1689	304.15601	2.070177
	Degraded forest	298.9621	311.1268	304.455889	2.375919
	Barren land	299.1291	310.4049	305.051061	2.253595
	Dense forest	298.9081	307.1801	302.08774	1.684755
	Waterbody	300.6923	308.0041	304.04645	1.601645
	Forest blank	299.4755	307.7154	302.673694	1.635159
	Settlement	300.0040894	309.8885	304.063018	1.792917
TLIVI	Open forest	0.94961226	1.014717	0.98808529	0.007615
	Fallow land	0.91483116	1.023605	0.99986207	0.008899
	Crop land	0.89946598	1.023543	0.99792403	0.007496
	Degraded forest	0.96659845	1.017884	0.99499643	0.007727
	Barren land	0.96406806	1.019268	1.00187808	0.0062
	Dense forest	0.95951813	1.00725	0.98329326	0.007765
	Waterbody	0.9610377	1.021617	1.00506566	0.011254
	Forest blank	0.9718318	1.008142	0.99253431	0.007649
	Settlement	0.96697211	1.012114	0.99750746	0.009046
ATLIVI	Open forest	0.94646335	1.01423	0.98641347	0.008462
	Fallow land	0.91234928	1.024805	1.00018511	0.010027
	Crop land	0.89682394	1.024387	0.99777345	0.008468
	Degraded forest	0.9634102	1.018028	0.99426335	0.008805
	Barren land	0.96033454	1.020677	1.00232151	0.007245
	Dense forest	0.95644742	1.008795	0.98123675	0.008378
	Waterbody	0.95786357	1.020321	1.00430187	0.011592
	Forest blank	0.96915913	1.00725	0.99150301	0.008618
	Settlement	0.96423066	1.014339	0.99740163	0.010104

gave the best results in terms of LULC classification accuracy. Table 3 shows the comparison of user's and producer's accuracy for every LULC classes for classifications using FCC and TLIVI as references which highlighted relative increase in accuracies for all the LULC categories, except for water bodies and open forest, which show neither increase nor decrease in the classification accuracy. The water bodies were already clearly discriminated from the original standard FCC image due to absence of spectral mixtures. Maximum proportion of the study area was dominated by open deciduous forests and there were very limited spectral mixtures; hence, the classification accuracy results did not show any alterations in this case. Maximum increase in the classification accuracy was obtained for fallow land, barren land, degraded forest and forest blank. Crop land, dense forest and settlements showed slight to marginal increase in the classification accuracy.

3.4. Statistical analysis

The average values of every land use-land covers of the study area corresponding to TLIVI and ATLIVI has been graphically represented in Fig. 7(a and b). This shows the variation of the different LULC categories in respect to the new indices under investigation in the study. This proves the potential of these two indices in LULC classification. The maximum, minimum, average and standard deviation values for every parameter are documented in Table 2. The graph shows unique variations of the parameters depending upon the LULC categories. Correlation, in terms of R^2 values was calculated between the derived ST and other associated parameters (Table 4). Results show fairly good correlation between LST and EVI2 ($R^2 = 0.83$) than to NDVI, SAVI and LAI ($R^2 = 0.5$–0.56). Hence, TLIVI developed using NDVI and LAI shows lesser correlation with ST of 0.65 than compared

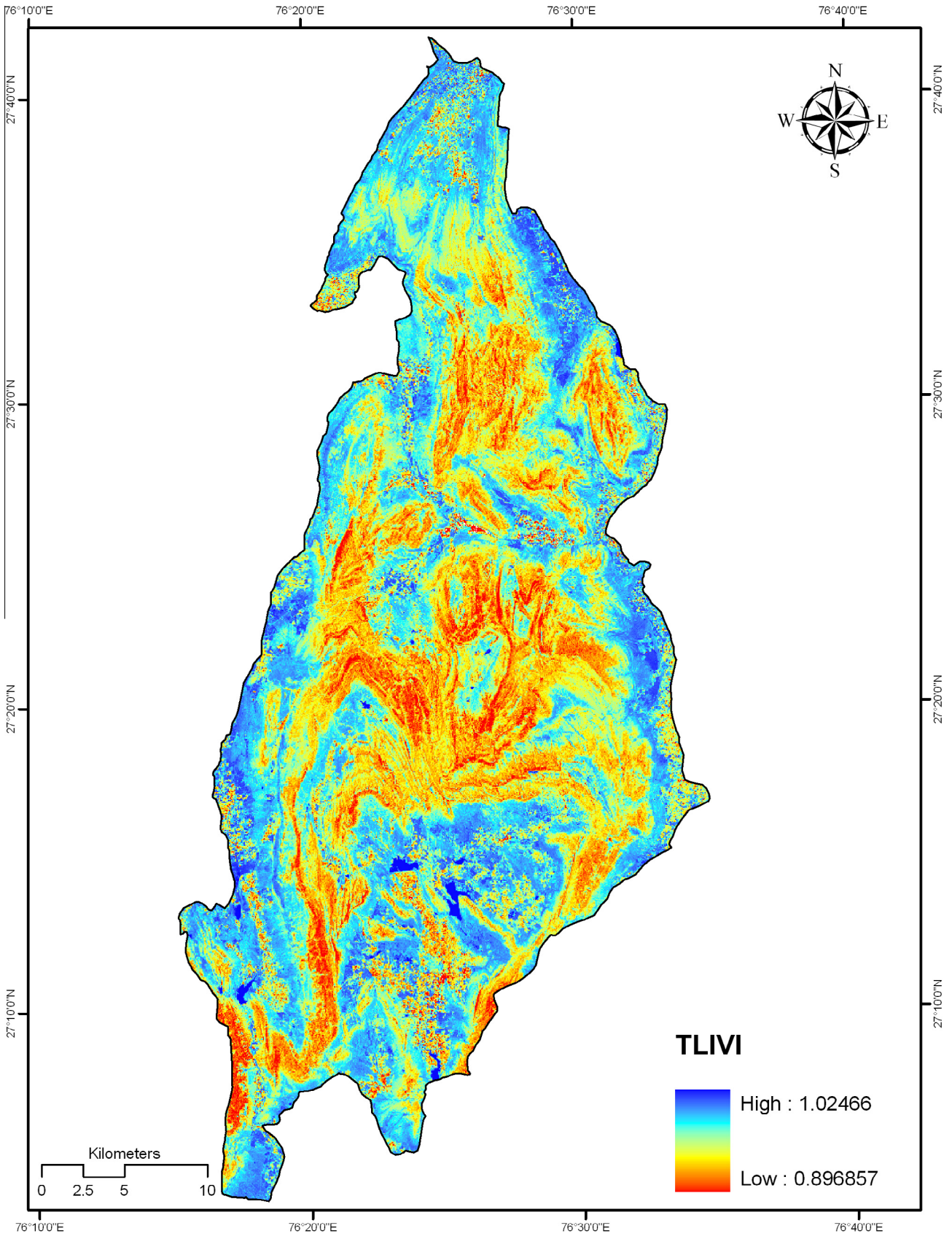

Figure 5 Thermal Vegetation Index maps: (a) Thermal Integrated Vegetation Index (TLIVI) map. (b) Advanced Thermal Integrated Vegetation Index (ATLIVI) map.

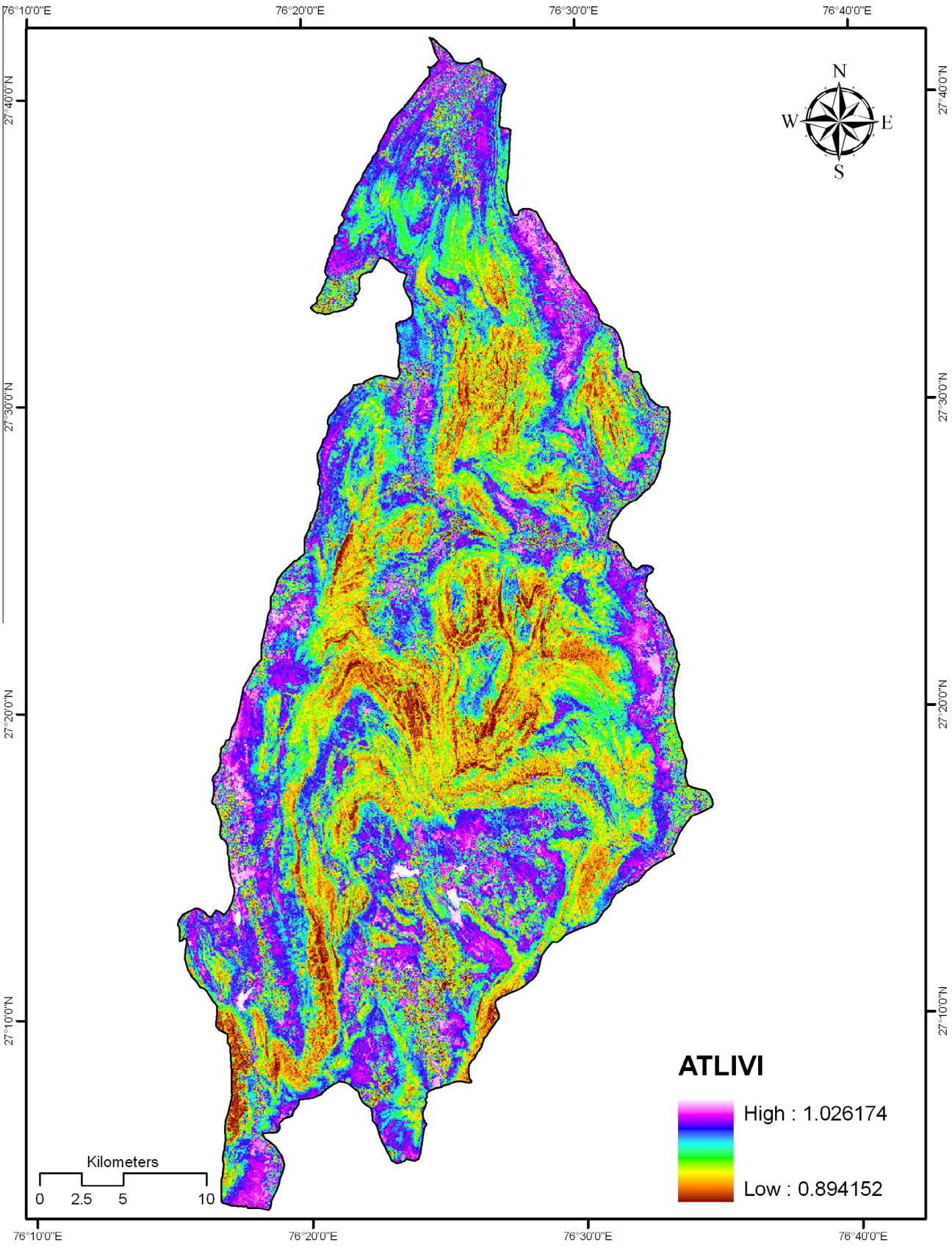

Fig. 5 (*continued*)

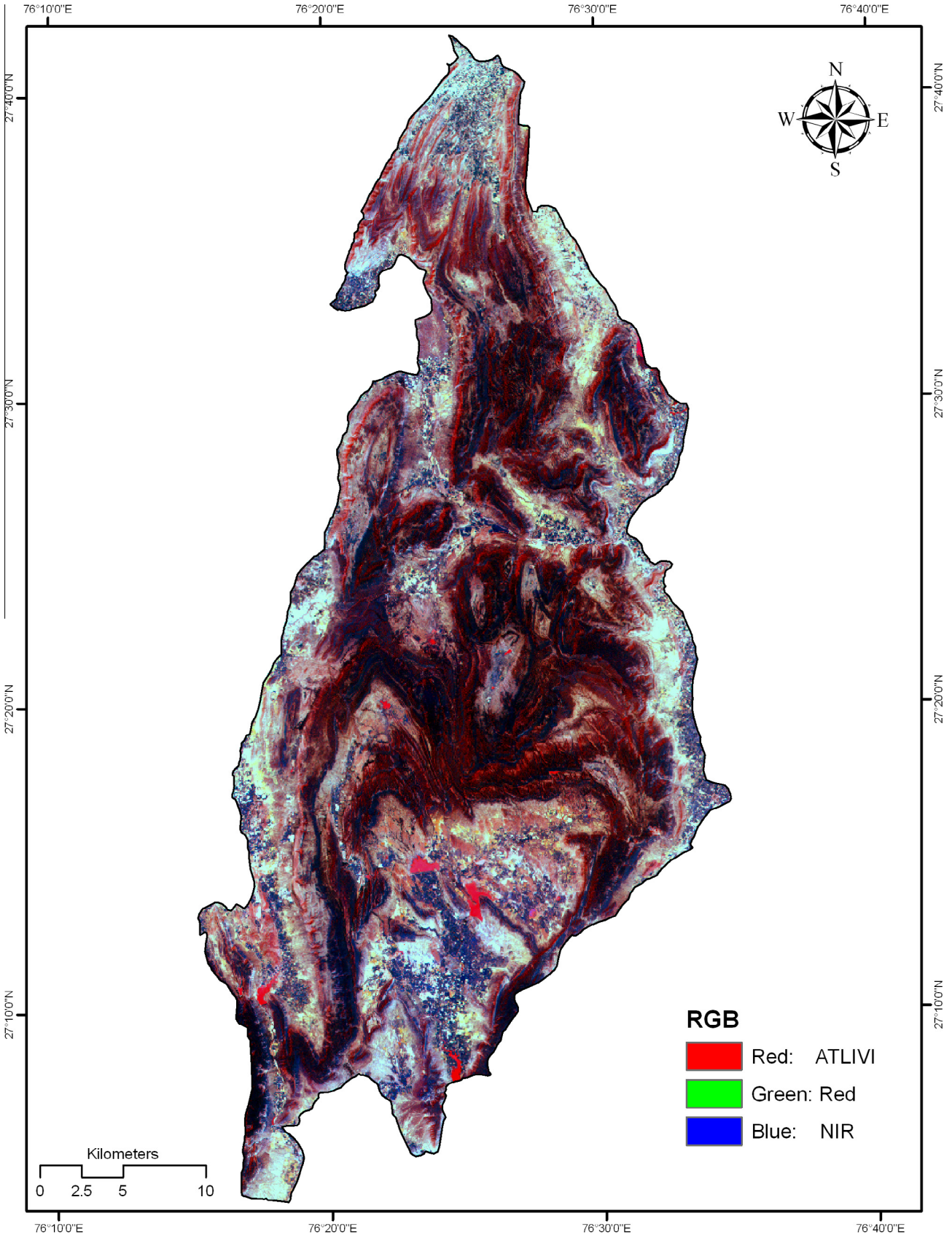

Figure 6 FCC with ATLIVI, Red and NIR in RGB channels.

Table 3 Classification accuracies.

Data used	Standard FCC		+TLIVI		+ATLIVI	
LULC	UA	PA	UA	PA	UA	PA
Fallow land	74.21	89.74	84.64	89.75	83.25	89.20
Barren land	85.02	93.52	92.01	95.30	93.77	96.43
Open forest	90.82	93.26	90.17	92.97	91.38	92.48
Degraded forest	75.62	85.08	90.33	92.75	91.42	93.13
Water body	99.97	99.88	99.97	99.91	99.97	99.91
Settlement	65.79	61.40	69.18	61.99	70.43	64.18
Dense forest	77.86	72.61	78.90	81.98	79.04	92.88
Forest blank	47.29	52.21	56.25	58.37	57.05	59.96
Crop land	93.26	77.94	93.63	86.51	93.63	88.84
OA	0.8504 (= 85%)		0.9022 (= 90.2%)		0.9101 (= 91%)	
k	0.8063 (= 0.8)		0.8666 (= 0.86)		0.8772 (= 0.87)	

Note: UA = User Accuracy, PA = Producer Accuracy, OA = Overall Accuracy, k = Kappa coefficient.

Table 4 Correlation (R^2) statistics.

	LAI	SAVI	NDVI	F_c	TLIVI	EVI2	ATLIVI
LST	0.56	0.51	0.57	0.6	0.65	0.83	0.7
LAI		0.94	0.79	0.8	0.84	0.53	0.83
SAVI			0.89	0.89	0.88	0.45	0.85
NDVI				0.99	0.98	0.56	0.96
F_c					0.99	0.68	0.99
TLVI						0.61	0.98
EVI2							0.74

to ATLIVI (R^2 = 0.7) developed with an additional parameter of EVI2 apart from NDVI and LAI. As mentioned in Table 4, ATLIVI shows high correlation with all the parameters under consideration. Fractional vegetation cover also had fine correlations with all the above mentioned parameters, including the formulated thermal vegetation indices.

Several factors affect the retrieval of LST from satellite thermal infrared data likewise, transmittance, atmospheric moisture, radiance, etc. which are quite difficult to estimate from satellite remote observations. In this study, we selected only surface emissivity because it is an important factor affecting the retrieval of ST from thermal satellite imagery and can be estimated easily through remote sensing. In this study, emissivity being characterized by surface features was estimated in terms of NDVI and LAI; which were in-turn estimated through satellite observations. All these spectral vegetation indices varied spatially depending upon the spatial features on the land surface. LAI in-turn determined empirically from SAVI also considers the soil factor. Retrieval of surface temperature of heterogeneous tropical forests by Landsat ETM+ showed relatively low ranges of ST in the forested vegetative parts, which was quite obvious. Water bodies also help in the reduction of the radiation heat flux. Results indicated lower ST values as compared to barren areas. As the rural settlements were small and scattered in pockets within and around the forested regions, the temperatures were not that high. The area is not economically sound, hence the development in terms of paved roads or concrete structures is lacking. So, naturally the ST will be low as this is characterized by the surface features present. Henceforth, ST was high in areas of fallow and barren spaces. Generally, an inverse relation existed between LAI and surface albedo increases due to increased canopy absorption and decreased reflection from the generally brighter ground below the vegetation. However, this was not profoundly observed in this study. Fractional vegetation cover had a fairly good correlation with all the associated parameters including ST. Soil Moisture Index is a function of LST involving maximum and minimum surface temperature for a given NDVI. Values range from 0 at the dry edge to 1 at wet edge (maximum evapotranspiration). Hence, a potential area of study dealing with soil moisture and evapotranspiration exists with forest surface temperature.

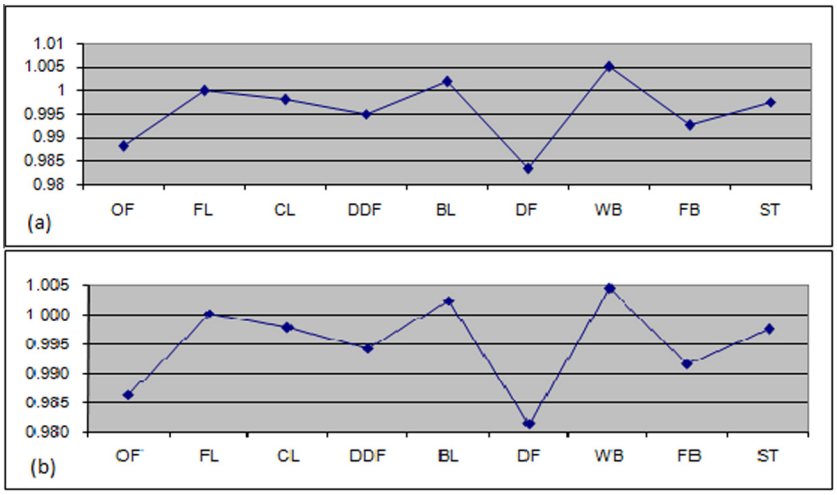

Figure 7 Variations in the average values for TLIVI and ATLIVI for every land-use land-cover categories (OF = open forest, FL = fallow land, CL = crop land, DDF = degraded forest, BL = barren land, DF = dense forest, WB = waterbody, FB = forest blank, ST = settlement). (a) Thermal Integrated Vegetation Index (TLIVI). (b) Advanced Thermal Integrated Vegetation Index (ATLIVI).

4. Conclusions

In summary, the method used to retrieve LST can be applied to achieve a quick prediction of LST from Landsat ETM + data using fewer parameters with reasonable accuracy. The method can be upscaled for larger areas; however, MODIS has unique applicability for a greater extent of the study area. For regional studies of LST, Landsat ETM + is probably the best choice. In addition to determining the forest canopy surface temperature (FST), the LST of a forest, ETM + thermal data can also be used to estimate the temperatures inside a forest, which is impossible with conventional methods.

In the study, the accuracy of classification is evaluated using thermal (TIR) information along with spectral (NIR, R) information generated from Landsat ETM + satellite imagery. Thermal Vegetation Index (TLIVI and ATLIVI) as proposed in the study helps to classify LULC more accurately (nearly 6% more) as compared to the satellite standard FCC RGB image. EVI2 has greater correlation with the ST derived as compared to other spectral vegetation indices adopted in the study. Hence, ATLIVI involving EVI2 with NDVI and LAI gives better correlation with ST than TLIVI that involves only NDVI and LAI and not EVI2. All the correlations could further increase if not the values for water bodies fluctuate a lot in the study area. Hence, these indices show lesser response to the water bodies. The study suggests the use of both NDVI and LAI instead of just NDVI in determining surface temperature and LULC classification. This improves further with the addition of EVI2 along with NDVI and LAI. Simultaneous inclusion of NDVI, SAVI, LAI and EVI2 has shown improvement in the classification probably by overcoming the saturation problem faced individually. Incorporating the thermal information along with these further enhanced the classification accuracy. The reason behind this is the integration of surface temperature regimes or the thermal information along with the vegetation and soil parameters for the analysis. The accuracy of classification is more profound in cases of fallow land, barren land, settlement, degraded forests and forest blank due to greater proportions of soil content, which is absent for water bodies. Hence, it can be concluded that the thermal indices (TLIVI and ATILVI) can very well distinguish between the vegetation and soil and thus, the indices are sensitive to vegetation-soil interactions; resulting in the improvement of the LULC classification accuracy. Therefore, the study recommends the use of thermal information along with spectral information from satellite data for better digital classification of LULC.

Acknowledgement

The authors are thankful to Department of Remote Sensing, Birla Institute of Technology, Mesra, India where the work has been done. Officials of Project Tiger, Sariska and Sariska Forest Division are thanked for their support.

References

Alavipanah, S.K., Saradjian, M., Savaghebi, Gh.R., Komaki, Ch.B., Moghimi, E., Reyhan, M.K., 2007. Land Surface Temperature in the Yardang region of Lut Desert (Iran) based on field measurements and Landsat thermal data. J. Agric. Sci. Technol. 9, 287–303.

Bastiaanssen, W.G.M., Menenti, M., Feddes, R.A., Holtslag, A.A. M., 1998. A remote sensing surface energy balance algorithm for land (SEBAL) 1. Formulation. J. Hydrol. 212, 198–212.

Bayala, M.I., Rivas, R.E., 2014. Enhanced sharpening procedures on edge difference and water stress index basis over heterogeneous landscape of sub-humid region. Egypt. J. Remote Sens. Space Sci. 17, 17–27.

Becker, F., Li, Z.-L., 1990. Temperature independent spectral indices in thermal infrared bands. Remote Sens. Environ. 32, 17–33.

Blaschke, T., 2010. Object based image analysis for remote sensing. ISPRS J. Photogramm. Remote Sens. 65, 2–16.

Buermann, W., Dong, J., Zeng, X., Myneni, R.B., Dickinson, R.E., 2001. Evaluation of the utility of satellite-based vegetation leaf area index data for climate simulations. J. Climate 14, 3536–3550.

Choudhury, B.J., Ahmed, N.U., Idso, S.B., Reginato, R.J., Daughtry, C.S.T., 1994. Relations between evaporation co-efficients and vegetation indices studied by model simulations. Remote Sens. Environ. 50, 1–17.

Dash, P., Göttsche, F., Olesen, F., Fischer, H., 2001. Retrieval of land surface temperature and emissivity from satellite data: physics, theoretical limitations and current methods. J. Indian Soc. Remote Sens. 29, 23–30.

Dash, P., Göttsche, F.M., Olesen, F.S., Fischer, H., 2002. Land surface temperature and emissivity estimation from passive sensor data: theory and practice-current trends. Int. J. Remote Sens. 23, 2563–2594.

Dousset, B., Gourmelon, F., 2003. Satellite multi-sensor data analysis of urban surface temperatures and landcover. ISPRS J. Photogramm. Remote Sens. 58, 43–54.

Duah, S.O., Donoghue, D.N.M., Burt, T.P., 2008. Intercomparison of evapotranspiration over the Savannah Voltu Basin in West Africa using remote sensing data. Sensors 8, 2736–2761.

El-Asmar, H.M., Hereher, M.E., El Kafrawy, S.B., 2013. Surface area change detection of the Burullus Lagoon, North of the Nile delta, Egypt, using water indices: a remote sensing approach. Egypt. J. Remote Sens. Space Sci. 16, 119–123.

Enderle, D., Weih Jr., R.C., 2005. Integrating supervised and unsupervised classification methods to develop a more accurate land cover classification. J. Ark. Acad. Sci. 59, 65–73.

Fan, L., Liu, Sh., Bernhofer, Ch., Liu, H., Berger, F.H., 2007. Regional land surface energy fluxes by satellite remote sensing in the Upper Xilin River Watershed (Inner Mongolia, China). Theor. Appl. Climatol. 88, 231–245.

Faris, A.A., Reddy, Y.S., 2010. Estimation of urban heat island using Landsat ETM + imagery at Chennai city – a case study. Int. J. Earth Sci. Eng. 3, 332–340.

Galve, J.M., Coll, C., Caselles, V., Valor, E., Niclòs, R., Sànchez, J. M., Mira, M., 2007. Simulation and validation of land surface temperature algorithms for MODIS and AATSR data. Tethys 4, 27–32.

Glenn, E.P., Huete, A.R., Nagler, P.L., Nelson, S.G., 2008. Relationship between remotely-sensed vegetation indices, canopy attributes and plant physiological processes: what vegetation indices can and cannot tell us about the landscape. Sensors 8, 2136–2160.

Hachem, S., Duguay, C.R., Allard, M., 2012. Comparison of MODIS-derived land surface temperatures with ground surface and air temperature measurements in continuous permafrost terrain. Cryosphere 6, 51–69.

Hales, K., Neelin, J.D., Zeng, N., 2004. Sensitivity of tropical land climate to leaf area index: role of surface conductance versus albedo. J. Climate 17, 1459–1473.

Hanes, J.M., Schwartz, M.D., 2011. Modeling land surface phenology in a mixed temperate forest using MODIS measurements of leaf area index and land surface temperature. Theor. Appl. Climatol. 105, 37–50.

Huete, A.R., Didan, K., Miura, T., Rodriguez, E.P., Gao, X., Ferreira, L.G., 2002. Overview of the radiometric and biophysical

performance of the MODIS vegetation indices. Remote Sens. Environ. 83, 195–213.
Huete, A.R., Liu, H.Q., Batchily, K., van Leeuwen, W.J.D., 1997. A comparison of vegetation indices over a global set of TM images for EOS-MODIS. Remote Sens. Environ. 59, 440–451.
Hussain, A., Bhalla, P., Palria, S., 2014. Remote sensing based analysis of the role of land use/land cover on surface temperature and temporal changes in temperature: a case study of Ajmer district. Int. Arch. Photogram. Rem. Sens. Spatial Inform. Sci, XL-8. Hyderabad, India, http://dx.doi.org/10.5194/isprsarchives-XL-8-1447-2014.
Iqbal, M.F., Khan, I.A., 2014. Spatiotemporal land use land cover change analysis and erosion risk mapping of Azad Jammu and Kashmir, Pakistan. Egypt. J. Remote Sens. Space Sci. 17, 209–229.
Jenerette, G.D., Harlan, S.L., Brazel, A., Jones, N., Larsen, L., Stefanov, W.L., 2007. Regional relationships between surface temperature, vegetation, and human settlement in a rapidly urbanizing ecosystem. Landscape Ecol. 22, 353–365.
Jiang, Z., Huete, A.R., Didan, K., Miura, T., 2008. Development of a two-band enhanced vegetation index without a blue band. Remote Sens. Environ. 112, 3833–3845.
Jin, M., Zhang, D.-L., 2002. Observed variations of leaf area index and its relationship with surface temperatures during warm seasons. Meteorol. Atmos. Phys. 80, 117–129.
Julien, Y., Sobrino, J.A., Mattar, C., Ruescas, A.B., Jiménez-munõz, J.C., Soria, G., Hidalgo, V., Atitar, M., Franch, B., Cuenca, J., 2011. Temporal analysis of normalized difference vegetation index (NDVI) and land surface temperature (LST) parameters to detect changes in the Iberian land cover between 1981 and 2001. Int. J. Remote Sens. 32, 2057–2068.
Karnieli, A., Agam, N., Pinker, R.T., Anderson, M., Imhoff, M.L., Gutman, G.G., Panov, N., Goldberg, A., 2010. Use of NDVI and land surface temperature for drought assessment: merits and limitations. J. Climate 23, 618–633.
Kaufmann, R.K., Zhou, L., Myneni, R.B., Tucker, C.J., Slayback, D., Shabanov, N.V., Pinzon, J., 2003. The effect of vegetation on surface temperature: a statistical analysis of NDVI and climate data. Geophys. Res. Lett. 30, 2147. http://dx.doi.org/10.1029/2003GL018251.
Kumar, P., Singh, B.K., Rani, M., 2013. An efficient hybrid classification approach for land use/land cover analysis in a semi-desert area using ETM + and LISS-III sensor. IEEE Sens. J. 13 (6), 2161–2165.
Lambin, E.F., Ehrlich, D., 1995. Combining vegetation indices and surface temperature for land-cover mapping at broad spatial scales. Int. J. Remote Sens. 16, 573–579.
Lambin, E.F., Ehrlich, D., 1996. The surface temperature-vegetation index space for land cover and land-cover change analysis. Int. J. Remote Sens. 17, 463–487.
Landsat Project Science Office, 2002. Landsat 7 science data user's handbook. Goddard Space Flight Center. Available from: < http://ltpwww.gsfc.nasa.gov/IAS/handbook/handbook_toc.html > .
Li, F., Jackson, T.J., Kustas, W.P., Schmugge, T.J., French, A.N., Cosh, M.H., Bindlish, R., 2004. Deriving land surface temperature from Landsat 5 and 7 during SMEX02/SMACEX. Remote Sens. Environ. 92, 521–534.
Li, H., Zhang, S., Sun, Y., Gao, J., 2011. Land cover classification with multi-source data using evidential reasoning approach. Chin. Geog. Sci. 21 (3), 312–321.
Lillesand, T.M., Kiefer, R.W., 2003. Remote Sensing and Image Interpretation. John Wiley & Sons Inc, New York.
Liu, H.Q., Huete, A., 1995. A feedback based modification of the NDVI to minimize canopy background and atmospheric noise. IEEE Trans. Geosci. Remote Sens. 33, 457–465.
Mallick, J., Kant, Y., Bharath, B.D., 2008. Estimation of land surface temperature over Delhi using Landsat-7 ETM + . J. Indian Geophys. Union 12, 131–140.
Mildrexler, D.J., Zhao, M., Running, S.W., 2011. A global comparison between station air temperatures and MODIS land surface temperatures reveals the cooling role of forests. J. Geophys. Res. 116, G03025. http://dx.doi.org/10.1029/2010JG001486.
NASA, 2008. Landsat-7 Science Data Users Handbook, chapter 11. Available from: < http://Landsathandbook.gsfc.nasa.gov/handbook.html > .
NASA, 2009. Landsat 7 Science Data Users Handbook, Chapter 2. 11:117-120. Available from: < http://Landsathandbook.gsfc.nasa.gov/handbook.html > .
Nizalapur, V., 2008. Land cover classification using multi-source data fusion of ENVISAT-ASAR and IRS P6 LISS-III satellite data – a case study over tropical moist deciduous forested regions of Karnataka, India. Int. Arch. Photogram. Rem. Sens. Spatial Inform. Sci. XXXVII (Part B6b), Beijing, China.
Oberg, J.W., Assefa, A.M., 2006. Evapotranspiration dynamics at an ecohydrological restoration site: an energy balance and remote sensing approach. J. Am. Water Resour. Assoc. 42, 565–582.
Owen, T.W., Carlson, T.N., Gillies, R.R., 1998. Remotely sensed surface parameters governing urban climate change. Int. J. Remote Sens. 19, 1663–1681.
Peña, M.A., 2009. Examination of the land surface temperature response for Santiago, Chile. Photogramm. Eng. Remote Sens. 75, 1191–1200.
Pinheiro, A.C.T., Descloitres, J., Privette, J.L., Susskind, J., Iredell, L., Schmaltz, J., 2007. Near-real time retrievals of land surface temperature within the MODIS Rapid Response System. Remote Sens. Environ. 106, 326–336.
Prata, A.J., Caselles, V., Coll, C., Sobrino, J., Ottle, C., 1995. Thermal remote sensing of land surface temperature from satellites: current status and future prospects. Remote Sens. Rev. 12, 175–224.
Price, J.C., 1989. Quantitative aspects of remote sensing in the thermal infrared. In: Asrar, G. (Ed.), Theory and applications of optical remote sensing, New York.
Rawat, J.S., Biswas, V., Kumar, M., 2013a. Changes in land use/cover using geospatial techniques: a case study of Ramnagar town area, district Nainital, Uttarakhand, India. Egypt. J. Remote Sens. Space Sci. 16, 111–117.
Rawat, J.S., Kumar, M., Biswas, V., 2013b. An integrated approach of Remote Sensing and GIS for land use/cover change detection: a case study of Bhimtal tourist town (India). Bull. Environ. Sci. Res. 2 (2–3), 1–6.
Rawat, J.S., Kumar, M., 2015. Monitoring land use/cover change using remote sensing and GIS techniques: a case study of Hawalbagh block, district Almora, Uttarakhand, India. Egypt. J. Remote Sens. Space Sci. 18, 77–84.
Sandholt, I., Rasmussen, K., Andersen, J., 2002. A simple interpretation of the surface temperature/vegetation index space for assessment of surface moisture status. Remote Sens. Environ. 79, 213–224.
Setturu, B., Rajan, K.S., Ramachandra, T.V., 2013. Land surface temperature responses to land use land cover dynamics. Geoinfor. Geostat. 1 (4). http://dx.doi.org/10.4172/2327-4581.1000112.
Sharma, L.K., Pandey, P.C., Nathawat, M.S., 2012. Assessment of land consumption rate with urban dynamics change using geospatial techniques. J. Land Use Sci. 7, 135–148.
Sharma, L.K., Nathawat, M.S., Sinha, S., 2013. Top-down and bottom-up inventory approach for above ground forest biomass and carbon monitoring in REDD framework using multi-resolution satellite data. Environ. Monit. Assess. 185, 8621–8637.
Sims, D.A., Rahman, A.F., Cordova, V.D., El-Masri, B.Z., Baldocchi, D.D., Bolstad, P.V., Flanagan, L.B., Goldstein, A.H., Hollinger, D.Y., Misson, L., et al, 2008. A new model of gross primary productivity for North American ecosystems based solely on the enhanced vegetation index and land surface temperature from MODIS. Remote Sens. Environ. 112, 1633–1646.
Sinha, S., 2015. Integrated geospatial technology for appraising surface temperature and forest biomass in context to conducive

tiger habitats in Sariska Wildlife Reserve, India. Res. Rev.: J. Space Sci. Tech. 4 (1), 8–14.

Sinha, S., Pandey, P.C., Sharma, L.K., Nathawat, M.S., Kumar, P., Kanga, S., 2014. Remote estimation of land surface temperature for different LULC features of a moist deciduous tropical forest region. In: Srivastava, P.K., Mukherjee, S., Gupta, M., Islam, T. (Eds.), . In: Remote Sensing Applications in Environmental Research (Part 1). Springer International Publishing, Switzerland. http://dx.doi.org/10.1007/978-3-319-05906-8_4.

Sinha, S., Sharma, L.K., Nathawat, M.S., 2011a. Retrieving tiger habitats: conserving wildlife geospatially. Appl. Remote Sens. J. 2, 1–5.

Sinha, S., Sharma, L.K., Pandey, P.C., Nathawat, M.S., Kanga, S., 2011b. Impact of human intrusion on tiger habitat and conservation using integrated geospatial techniques. Int. J. Earth Sci. Eng. 4, 39–45.

Sinha, S., Sharma, L.K., 2013. Investigations on potential relationship between biomass and surface temperature using thermal remote sensing over tropical deciduous forests. Res. Rev.: J. Space Sci. Tech. 2 (3), 13–18.

Snyder, W.C., Wan, Z., Zhang, Y., Feng, Y.Z., 1998. Classification based emissivity for land surface temperature measurement from space. Int. J. Remote Sens. 19, 2753–2774.

Sobrino, J.A., El Kharraz, J., Li, Z.L., 2003. Surface temperature and water vapour retrieval from MODIS data. Int. J. Remote Sens. 24, 5161–5182.

Stathopoulou, M., Cartalis, C., 2007. Daytime urban heat islands from Landsat ETM + and Corine land cover data: an application to major cities in Greece. Sol. Energy 81, 358–368.

Sun, D., Kafatos, M., 2007. Note on the NDVI-LST relationship and the use of temperature-related drought indices over North America. Geophys. Res. Lett. 34, L24406. http://dx.doi.org/10.1029/2007GL031485.

Tomlinson, C.J., Chapman, L., Thornes, J.E., Baker, C., 2011. Remote sensing land surface temperature for meteorology and climatology: a review. Meteorol. Appl. 18, 296–306.

van Leeuwen, T.T., Frank, A.J., Jin, Y., Smyth, P., Goulden, M.L., van der Werf, G.R., Randerson, J.T., 2011. Optimal use of land surface temperature data to detect changes in tropical forest cover. J. Geophys. Res. 116, G02002. http://dx.doi.org/10.1029/2010JG001488.

Wan, Z., Wang, P., Li, X., 2004. Using MODIS land surface temperature and normalized difference vegetation index products for monitoring drought in the southern Great Plains, USA. Int. J. Remote Sens. 25, 61–72.

Wang, W., Huang, D., Wang, X.-G., Liu, Y.-R., Zhou, F., 2011. Estimation of soil moisture using trapezoidal relationship between remotely sensed land surface temperature and vegetation index. Hydrol. Earth Syst. Sci. 15, 1699–1712.

Wen, J., Su, Z., Ma, Y., 2003. Determination of land surface temperature and soil moisture from Tropical Rainfall Measuring Mission/Microwave Imager remote sensing data. J. Geophys. Res. 108 (D2), 4038. http://dx.doi.org/10.1029/2002JD002176.

Weng, Q., 2009. Thermal infrared remote sensing for urban climate and environmental studies: methods, applications, and trends. ISPRS J. Photogramm. Remote Sens. 64, 335–344.

Weng, Q., Lu, D., Schubring, J., 2004. Estimation of land surface temperature-vegetation abundance relationship for urban heat island studies. Remote Sens. Environ. 89, 467–483.

Weng, Q., Yang, S., 2006. Urban air pollution patterns, land use and thermal landscape: an examination of the linkage using GIS. Environ. Monit. Assess. 117, 463–489.

Wu, C., Niu, Z., 2012. Modelling light use efficiency using vegetation index and land surface temperature from MODIS in Harvard Forest. Int. J. Remote Sens. 33, 2261–2276.

Yue, W., Xu, J., Tan, W., Xu, L., 2007. The relationship between land surface temperature and NDVI with remote sensing: application to Shanghai Landsat 7 ETM + data. Int. J. Remote Sens. 28, 3205–3226.

Zhang, X.Y., Friedl, M.A., Schaaf, C.B., Strahler, A.H., Hodges, J.C. F., Gao, F., Reed, B.C., Huete, A., 2003. Monitoring vegetation phenology using MODIS. Remote Sens. Environ. 84, 471–475.